Research Article

Journal of Environmental Nanotechnology

Chavibetol-Loaded Zinc Oxide Nanoparticles for Enhanced Anticancer Applications against A549 Human Lung Cancer Cells

Balaji Murugesan, Rajesh Pattulingam* and Syed Illiyas Syed Maqbool

PG and Research Department of Chemistry, Government Arts College, Coimbatore, TN, India

Received: 21.09.2024 Accepted: 14.12.2024 Published: 30.12.2024

*gacchemistryrajesh@gmail.com

ABSTRACT

Chavibetol-loaded zinc oxide nanoparticles (CB-ZnONPs) have demonstrated exceptional anticancer activity. The current study focuses on examining the synthesis of biocompatible zinc oxide nanoparticles infused with chavibetol. These nanoparticles were assessed for their ability to load and release chavibetol as a prodrug. Furthermore, the loaded particles were assessed for their ability to inhibit cell growth and induce programmed cell death in human lung cancer cell line (A549). The structure and morphological properties of the produced material were analyzed by scanning electron microscopy (SEM), Fourier transform infrared (FTIR) spectroscopy, X-ray diffraction analysis, dynamic light scattering analysis (DLS), and zeta potential analysis. Dynamic light scattering and scanning electron microscopy examination attest that the synthesized CB-ZnONPs have a size of around 50-60 nm. Furthermore, the analysis confirms that the nanoparticles possess a highly crystalline structure and exhibit a rod shape. The FTIR measurement confirms the conjugation of chavibetol molecules with zinc oxide nanoparticles. The X-ray diffraction patterns reveal that the zinc oxide nanoparticles possess a spinel structure and exhibit a high level of purity. Chavibetol-loaded nanoparticles exhibit a regulated release pattern in accordance with different pH levels. A notable suppression of cell growth in the group that received treatment was observed, followed by the occurrence of programmed cell death as indicated by the study of fluorescence microscopy using AO/EtBr. The synthesized material also showed that upregulation of apoptotic protein and down regulation of the antiapoptotic protein. The results of the study clearly show that chavibetol-loaded zinc oxide nanoparticles may effectively transport the desired drug and induce programmed cell death in specific human lung cancer cells.

Keywords: Zinc oxide nanoparticles; Chavibetol; Human lung cancer; Drug release; Protein expression; Apoptosis.

1. INTRODUCTION

According to a report by the World Health Organization (WHO), cancer was responsible for 10 million deaths in 2020, making it a leading cause of death and a major obstacle to increasing life expectancy. By 2040, it is estimated that there will be around 29.5 million new instances of cancer diagnosed annually, with an expected 16.4 million deaths attributable to cancer each year. Despite the implementation of innovative medical treatments and technological developments, cancer continues to be one of the most deadly diseases (Shah *et al.* 2019). It is a pathological condition defined by the proliferation of cells beyond normal control. Cancer cells typically reside in the body and perform similar functions to normal cells. Cancer occurs when unregulated cellular replication results in abnormal and excessive growth of cells. Cancer cells possess the capacity to develop their own vascular network, detach from the primary organ, move and disseminate to other organs in the body. If proliferation is not controlled and allowed to continue and spread, it can be deadly (Kulothungan *et al.* 2022).

This is mostly because cancer cells have the ability to disregard signals, while normal cells only multiply in response to signals. It could also be attributed to genetic variations that provide control points for cell growth. Cancer can also be caused by genomic instability, which refers to an increased occurrence of changes in the genome during the whole life cycle of dividing cells. Angiogenesis is another process by which cancer advances, resulting in the formation of new blood vessels to provide metastatic cancer cells with the necessary nutrition and oxygen (Tran *et al.* 2021). Cancer

does not arise from a singular causative element. The initiation of cancer is influenced by a multitude of internal and environmental variables. Internal variables encompass genetic abnormalities, genetic diseases, and hormone imbalances, whereas external causes encompass exposure to radiation, starvation, infectious agents, and tobacco use. Metastasis, often known as tumor dissemination, is responsible for approximately 90% of cancer-related fatalities (Pang *et al.* 2006; Nishida *et al.* 2006).

In recent years, scientists have become interested in nanoparticles (NPs) because of their notable effectiveness and safety. In recent years, nanotechnology-based therapeutic and diagnostic approaches have demonstrated significant potential in enhancing cancer therapy. Nanomedicine technologies have facilitated the development of innovative cancer treatments by enabling the encapsulation of therapeutic chemicals in nanoparticulate materials and their targeted delivery to tumors through passive permeation and active internalization mechanisms. The utilization of nanoparticles for therapeutic applications has been discovered to effectively reduce resistance, hence tackling a major challenge in traditional therapy. Research works are performed to discover more accurate nanotechnology-driven cancer therapies that exhibit less detrimental effects compared to traditional treatments (Baranwal *et al.* 2023). The advancement of nanomedicine technology has led to the availability of several cancer treatment nanomedicines in the market. Additionally, numerous nanomedicines employing different nanosystems such as metallic nanoparticles, liposomes, quantum dots, carbon nanotubes, polymeric micelles, and nanospheres are currently in advanced stages of development and clinical testing (Alrushaid *et al.* 2023). Zinc oxide nanoparticles (ZnO-NPs) are extensively used in drug delivery, cancer diagnostics, and treatment because of their distinct physical and chemical characteristics. ZnO-NPs have demonstrated effectiveness not only in cancer treatment but also in addressing a wide range of other applications across sectors such as cosmetics, electronics, and textiles. ZnO-NPs can be generated using chemical, physical, or biological methods. Precipitation, microemulsion, chemical reduction, sol-gel, and hydrothermal techniques are among the chemical methods that necessitate significant energy consumption and the maintenance of high pressure or temperature during the synthesis process (Anjum *et al.* 2021). They can also be produced *via* physical techniques such as vapor deposition, plasma, and ultrasonic irradiation, which are less frequently used compared to chemical procedures. However, these methods generally need a significant amount of energy and large machinery, resulting in increased costs for the items. Biological synthesis is an alternative approach for producing ZnO-NPs that is considered to be more environmentally friendly. Regardless of the approach used, all forms of ZnO nanoparticles have demonstrated effectiveness in addressing cancer through their ability to diagnose, treat, and deliver anticancer drugs in a sustained and focused manner (Aljabali *et al.* 2022). Zinc oxide nanoparticles are extensively utilized in various industries and research organizations due to their large range of applications. Due to the minute particle size of nano-ZnO, zinc can be readily absorbed by the human body. Due to its cost-effectiveness and lower toxicity compared to other metal oxide nanoparticles, ZnO-NPs have diverse applications in medicine, such as antibacterial, anti-diabetic, anti-inflammatory, anti-aging, wound healing, and bio-imaging (Jin *et al.* 2019).

Various inorganic metal oxides, including TiO_2, CuO, and ZnO, have been synthesized and are currently being studied. Among these metal oxides, ZnO-NPs are particularly intriguing because of their affordability, safety, and ease of preparation. Moreover, any agent designed for human ingestion for the purpose of treating specific disorders must possess the following properties. The substance should be non-toxic, inert towards food and the container, possess a nice taste or be devoid of taste, and not emit an unpleasant odor (Asif *et al.* 2023). ZnO-NPs are an example of an inorganic metal oxide that fulfills all the specified requirements, making them suitable for usage as a medicine, package preservative, and antibacterial agent without any safety concerns. Therefore, the US Food and Drug Administration (FDA) has categorized ZnO-NPs as a "GRAS" (generally regarded as safe) chemical. ZnO-NPs possess a significant band gap of 3.37 eV and a high exciton binding energy of 60 meV. As a result, they exhibit a diverse spectrum of semiconducting properties, such as robust catalytic activity, optical characteristics, UV filtering capabilities, anti-inflammatory effects, and wound healing properties. Additionally, they have been extensively utilized in cosmetic products, such as sunscreen creams, owing to their exceptional UV filtering properties. ZnO-NPs were initially employed in the rubber sector to enhance the durability of rubber composites, strengthen high polymers, and provide anti-aging characteristics. ZnO-NPs have garnered interest in the field of biological imaging because of their capacity to display luminescence. In addition, they have also

garnered the attention of researchers who are interested in developing diagnostic tools, as they can also be utilized in biosensing applications (Siddiqi *et al.* 2018).

Chavibetol is an organic substance belonging to the phenylpropanoid class. It is a major component of the essential oil derived from the leaves of the betel plant (*Piper betel*) and catania (Aara *et al.* 2020). This substance is a fragrant chemical that emits a pungent scent. Porous ZnO structures, including porous nanotubes, porous nanobelts, porous nanorods, and porous cages, have been effectively employed in targeted drug delivery systems. To ensure efficient drug delivery, the surface of nanoparticles can be modified through the use of different agents such as ligands, linker chains, medicines, and markers. Nanoparticles aggregate in cells by engaging in certain molecular interactions, such as receptor-ligand interactions. Upon receiving a suitable stimulus, the nanoparticles undergo endo/lysosomal escape and release the drug, leading to the destruction of its intended target. Different forms of internal and exterior stimuli are also involved in the precise administration of anticancer medications (Martínez *et al.* 2018).

The objective of this study was to synthesize zinc oxide nanoparticles using a hydrothermal approach, while being able to adjust the parameters and improve their biocompatibility. In addition, their typical drug encapsulation and release capabilities were assessed, taking into account their response to different pH levels in the system. Furthermore, chavibetol-loaded zinc oxide nanoparticles were synthesized and analyzed to investigate their potential as anticancer agents in lung cancer cells.

2. MATERIALS AND METHODS

Zinc nitrate, sodium hydroxide, methanol and ethanol were purchased from Merck Life Science Pvt. Ltd. Mumbai, India. Chavibetol was purchased from Sigma Aldrich Bengaluru, India. Cell culture media, MTT [3-(4,5-dimethyl-2-thiazolyl) 2,5 diphenyl-2-H-tetrazoliumbromide] and Dulbecco's modified eagle medium-high glucose (DMEM-HG) were acquired from Hi-Media Laboratories Pvt. Ltd, Mumbai, India. Acetone, DMSO, ascorbic acid and DPPH (2,2-diphenyl-1-picryl-hydrazyl) were acquired from Thomas Baker India. The cell line used in this study was acquired from the National Centre for Cell Science (NCCS), Pune, India. All chemicals were used in their original form. Double distilled water was used in all experiments.

2.1 Synthesis of ZnO Nanoparticles

ZnO nanoparticles were synthesized by hydrothermal technique. Zinc nitrate (0.1 M) and methanol (50 mL) were mixed in a beaker under continuous stirring at room temperature for 60 min. Subsequently, 0.4 M NaOH solution (25 mL) was added in a dropwise manner with continuous stirring. The mixture was then heated at 180 ℃ for 12h in an autoclave made of stainless steel and equipped with a Teflon-lined chamber. The solution was then allowed to cool at room temperature. The precipitate formed inside the Teflon chamber was then filtered and washed several times with distilled water and absolute methanol. The final product was dried in an oven at 60 ℃.

2.2 Synthesis of CB-ZnO Nanoparticles

Chavibetol-loaded ZnO nanoparticles (CB-ZnONPs) were synthesized as per previously reported method with minor modification. Briefly, 500 mg chavibetol was dissolved in 50 mL of 0.001 N NaOH solution and the required amount (100 mg) of ZnO nanoparticle was added into the chavibetol solution with constant stirring for 60 min at 80 ℃ to obtain a homogeneous mixture. Later, this homogeneous mixture was sonicated for 180 min to form the chavibetol-loaded ZnO nanoparticles. The obtained nanoparticles (CB-ZnO-NPs) were centrifuged and washed using ethanol and dried in the oven at 60 ℃.

2.3 FT-IR Characterization

Fourier transforms infrared (FT-IR) spectroscopy of CB-ZnONPs was performed using Nicolet 5700 instrument (Nicolet Instrument, Thermo Company, USA) with KBr pellet method. Each KBr disk was scanned over the 4000-500 cm^{-1}wave number region.

2.4 X-Ray Diffraction Analysis

The method of X-ray diffraction (XRD) was used to investigate the crystalline structure of CB-ZnO-NPs. The scanning rate employed was $1^{o}min^{-1}$ over the 10–80° 2θ range.

2.5 Zeta Potential Analysis

The zeta potential of the synthesized nanoparticles was determined by means of a zeta potential analyzer (90 Plus Particle Size Analyzer, Brookhaven Instruments Corporation, using Zeta Plus software).

2.6 Particle Size Analysis

The particle size range of the CB-ZnONPs along with its polydispersity was determined using a particle size analyzer (90 Plus Particle Size Analyzer, Brookhaven Instruments Corporation).

2.7 Scanning Electron Microscope (SEM) Analysis

For SEM analysis, the samples were placed on polycarbonate substrate and the excess water was left to dry at room temperature (JSM5600LV, JEOL, Japan) operating at an accelerating voltage of 20 kV.

2.8 Chavibetol Loading and Encapsulation Efficiency

Chavibetol (3 mg)-loaded ZnO nanoparticles were dispersed into 6 mL of phosphate buffer solution (PBS) and centrifuged at 12,000 rpm for 30 min. The supernatant was collected to measure the ultraviolet absorption at 280 nm. The loading efficiency and encapsulation efficiency of chavibetol-loaded ZnO nanoparticles were calculated as follows.

$$\text{Loading Efficiency} = W_0 / W \times 100\%$$

$$\text{Encapsulation Efficiency} = W_0/W_1 \times 100\%,$$

where, W_0 is the amount of chavibetol enveloped in the ZnO nanoparticles, W is the amount of ZnO-NPs nanoparticles, and W_1 is the amount of chavibetol added in the system.

2.9 In Vi*tro* Drug Release Study

The chavibetol-loaded nanoparticles were transferred to a beaker containing 100 mL of phosphate buffer (pH 5.5, 6.8 and 7.4) with continuous stirring at 100 rpm. The sink condition was maintained by periodically removing a 2-mL sample and replacing an equal volume of buffer. The amount of chavibetol release was analyzed with a spectrophotometer at 485 nm. The experiments were performed in triplicate for each of the samples.

2.10 Cell Viability Assay

Cell viability was determined by measuring the ability of cells to transform MTT to a purple formazan dye. Cells were seeded in 96-well tissue culture plates at 2×10^3 cells per well for 24 hours. The cells were then incubated with chavibetol, loaded and unloaded nanoparticles at different concentrations for different time periods. After treatment, 200 mL of MTT solution was added per well and incubated for another 5 hours. To dissolve the formazan salt formed, the medium was aspirated and replaced with 150 mL of DMSO per well. The cell growth conditions were recorded by the color intensity of the formazan solution. Absorbance at 570 nm was recorded on a 96-well microplate reader.

2.11 Morphological Study

The human lung cancer cells (A549) grown on coverslips (1×10^5 cells per coverslip) were incubated for 6-24 hours with compounds at the IC_{50} concentration, and they were then fixed in ethanol: acetic acid solution (3:1; v/v). The coverslips were gently mounted on glass slides for morphometric analysis. Three monolayers per experimental group were photomicrographed. The morphological changes of the selected cancer cells were analyzed using a Nikon (Japan) bright field inverted light microscope at 20x magnifications.

2.12 Fluorescence Microscopic Analysis of Cell Death

Approximately 1 mL of the dye mixture (100 mg/ mL acridine orange (AO) and 100 mg/mL ethidium bromide (EtBr) in distilled water) was mixed with 9 mL of cell suspension (1×10^4 cells per mL) on clean microscope coverslips. The cells were collected, washed with phosphate buffered saline (PBS) (pH 7.2) and stained with 1 mL of AO/EtBr. After incubation for 2 min, the cells were washed twice with PBS (5 min each) and visualized under a Fluorescence microscope (Nikon Eclipse, Inc, Japan) at 20x magnification with an excitation Filter at 480 nm. The same procedure was also followed for DAPI.

2.13 Protein Expression Analysis

The impact of CB-ZnONPs on apoptotic and anti-apoptotic proteins in both treated and untreated cells was determined by Western blotting. The PB-ZnONPs were incubated with the cells for 24 h in a 100 mm culture dish. The medium was then removed, and the analysis was performed.

3. RESULTS AND DISCUSSIONS

Chavibetol was selected as the model drug for targeted delivery into human cancer cells. Prior research has indicated that chavibetol has a significant role in the

proliferation of cancer cells. The overall functional efficacy of nanoparticle-based delivery systems is mostly determined by the physicochemical characteristics of the nanoparticles, including their size, shape, and physical state.

3.1 Encapsulation Efficiency

The chavibetol loading and encapsulation efficiency of zinc nanoparticles with different chavibetol concentrations was found to be proportional to the chavibetol concentration. The nanoparticles with 40 mg/mL of chavibetol showed highest encapsulation efficiency 88.6% respectively. Halanayake *et al.* (2021) defined particle entrapment efficiency as the percentage of ZnO-NPs entrapped within the chitosan shell relative to the initial amount used for encapsulation. The entrapment efficiency of ZnO-NPs synthesized using plant extract was evaluated. ZnO-NPs prepared with 0, 1, 5, 10, 15, and 20 mL of *Plumeria* extract exhibited efficiencies of 65%, 73%, 77%, 80%, 82%, and 82%, respectively. The maximum entrapment efficiency of 82% was observed for ZnO-NPs synthesized with 15 mL of plant extract, while the lowest value of 65% was recorded in the absence of plant extract. Entrapment efficiency increased with increasing extract concentration and reached a plateau at 15 mL. This trend may be attributed to the presence of bioactive compounds, such as plant alkaloids, which enhance interactions between the ZnO nanoparticle surface and chitosan molecules, thereby improving drug entrapment efficiency (DEE).

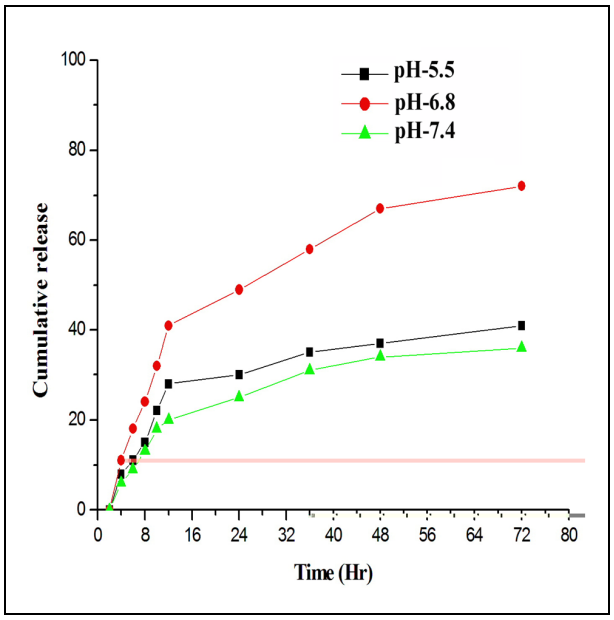


Fig. 1: Drug release study of CB-ZnO-NPs

3.2 Drug Release Study

The ability of the carrier to release the drug efficiently at the desired site is an important feature of any delivery system. Fig. 1 depicts the release of chavibetol from the zinc oxide nanoparticles in phosphate buffer (pH 7.4). At the end of 72 hours incubation, 74% of chavibetol was released in phosphate buffer. This revealed that the release of chavibetol was higher in acidic pH. This pH dependent release may help to improve the efficacy of chavibetol release into the system. This may initiate rapid release of chavibetol from the nanoparticles after internalization in the system. Such efficient release would ultimately result in improved anticancer activity against lung cancer system. It is evident that the drug is not released uniformly over the initial 7 hours at acidic pH values. Abayarathne *et al.* (2020) reported that at pH 5.0, the release of ZnO-NPs exhibits both increases and decreases, likely due to variations in nanoparticle porosity. Particles with higher porosity can accommodate greater amounts of cisplatin, contributing to a more uniform release profile. In contrast, at pH 6.0 and 4.0, the release of cisplatin remains nearly consistent, except for a brief fluctuation observed between 5 and 6 h at pH 6.0. At these pH levels, the nanoparticles demonstrate greater stability, and the release mechanism is predominantly governed by diffusion, resulting in a slow and sustained release of the encapsulated cisplatin.

3.3 FTIR

The functional groups of ZnO-NPs, chavibetol and CB-ZnO-NPs were investigated by FTIR technique. The FTIR spectrum (Fig. 2a) exhibited a broad peak at 3004 cm^{-1}, 2318 cm^{-1} due to the –OH stretching of the hydroxyl group, which arose due to the hygroscopic properties of ZnO-NPs. Small peaks between 752 cm^{-1} were due to -CH stretching mode of alkane groups. The most prominent characteristic peaks at 2255 and 1765 cm^{-1} were observed due to asymmetric and symmetric carboxylate stretching in chavibetol (Fig. 2b). A major peak was observed at 2496 cm^{-1} and 1374 (Fig. 2c) due to metal-oxygen (Zn-O) stretching. Li *et al.* (2015) reported that the PVA–Betel composite film exhibits all the characteristic absorption peaks of PVA (3294, 2920, and 1090 cm^{-1}) along with the betel leaf extract peak at 2360 cm^{-1}, with slight shifts and broadening. The shift of this peak from 2360 cm^{-1} to 2358 cm^{-1} was attributed to hydrogen bonding between the amine groups of betel leaf extract and the –OH groups of the PVA matrix, thereby supporting the present observations.

3.4 XRD

The XRD spectrum of CB-ZnO-NPs (Fig. 3) exhibited several characteristic peaks at 2θ=31.86, 34.31, 36.00 47.62, 56.74, 63.01, 68.20, 72.50 and 77.04, assigned to (100), (002), (101), (102), (110) (103) (112) (004) and (211) of ZnO nanoparticles. These results indicate that the structure of ZnO nanoparticle is polycrystalline in nature (JCPDS 50664). The XRD pattern of ZnONPs exhibited a broad peak at 2θ = 24.35° and some additional peaks of ZnO-NPs were also visible, confirming the presence of zinc as shown in Fig. 3a. The X-ray diffraction patterns of zinc oxide nanoparticles (ZnO-NPs) exhibited prominent and well-defined diffraction peaks, indicating a high degree of crystallization of the ZnO-NPs. The X-ray diffraction spectra confirmed the presence of the hexagonal (wurtzite) phase of crystalline ZnO, with a space group of lattice constants of a = 3.253 (Å) and c = 5.213 (Å). After loading with chavibetol the crystalline nature of particles still remains in such conditions (Fig. 3b). The XRD analysis did not detect any additional crystalline phases associated with contaminants, indicating that the synthesized ZnO-NPs have a high purity of the wurtzite phase. Moreover, the highest level of intensity observed in the ZnO-NPs sample occurred at an angle of 2θ = 36.275°, which corresponds to the (101) lattice associated with the wurtzite ZnO phase (Saddik *et al.* 2022).

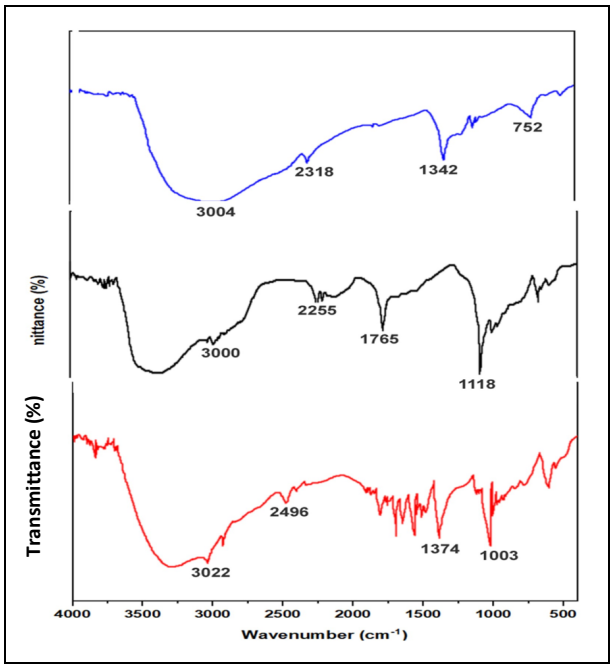


Fig. 2: FTIR spectrum of a) Zinc oxide NPs; b) Chavibetol and c) CB-ZnO-NPs

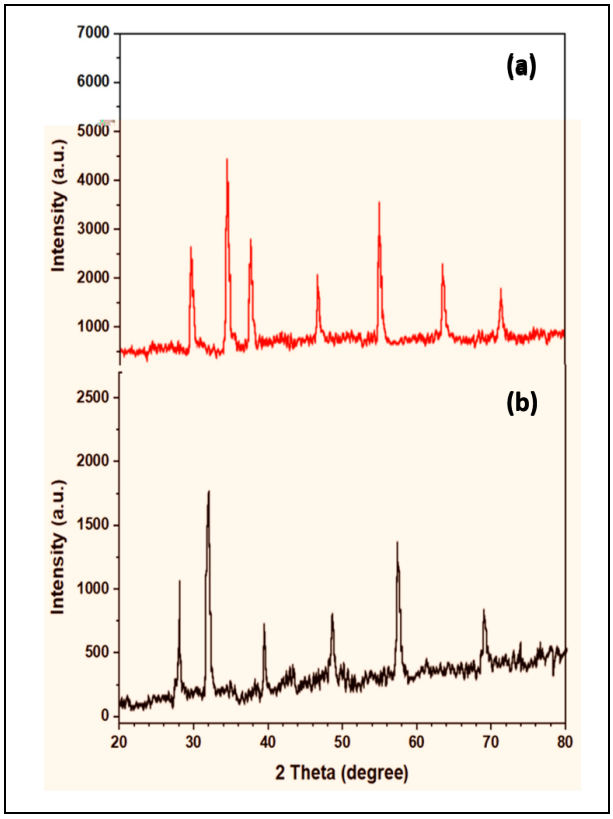


Fig. 3: XRD pattern of ZnONPs and CB-ZnO-NPs

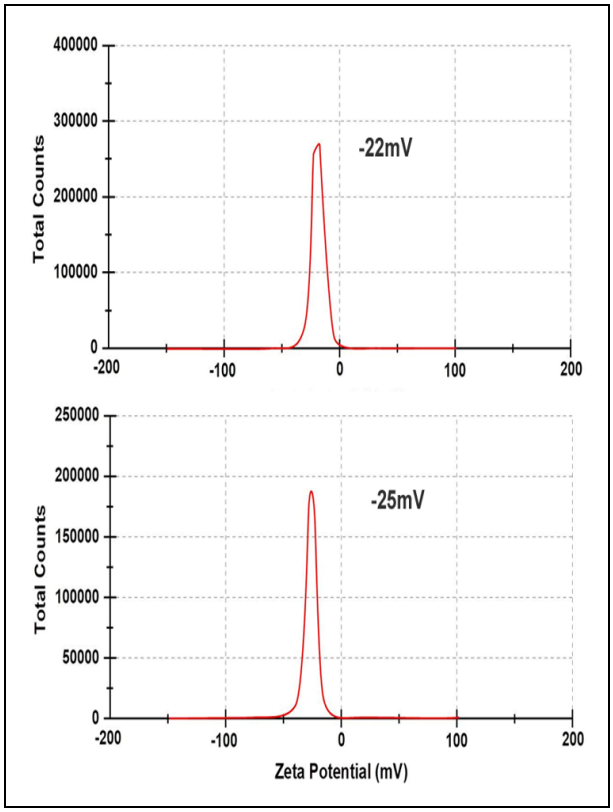


Fig. 4: Zeta potential distribution of ZnONPs and CB-ZnO-NPs

3.5 Zeta Potential and Particle Size Analysis

The zeta potential of CB-ZnO-NPs was -25 mV as shown in Fig. 4a, whereas that of the unloaded ZnO was 22 mV (Fig. 4b) indicating that chavibetol loaded ZnO nanoparticles were more stable as compared to ZnO nanoparticle due to the high charge repulsion between the nanoparticle (-30 mV charge is a sufficient charge to prevent accumulation and dispersed particle adhesion). The zeta potential conductivity and stability of ZnO-NPs increased after the coating of chavibetol, which is appropriate for the drug delivery application. The particle size of CB-ZnO-NPs was found to be in the range 46.5 nm to 70 nm.

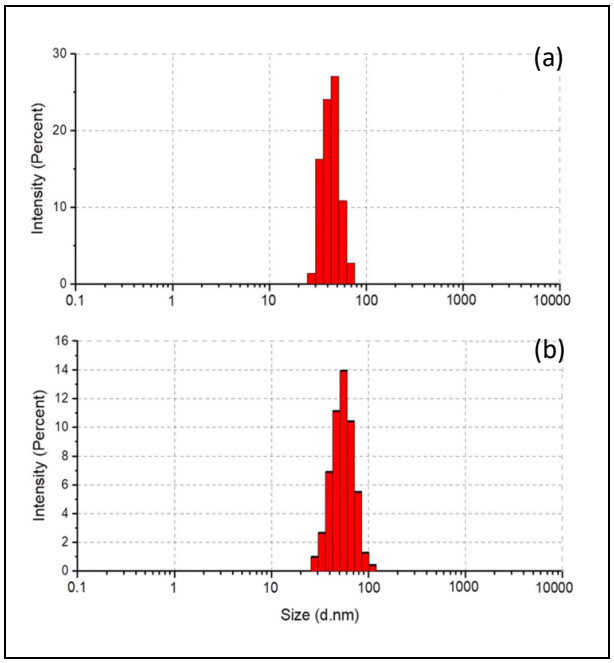


Fig. 5: DLS analyzer of ZnONPs and CB-ZnO-NPs

3.6 DLS

The average size of the CB-ZnO-NPs was determined using DLS measurement. The mean diameter for the green production of ZnO-NPs was 50 nm (Fig. 5a), and that of the chavibetol-loaded ZnO-NPs was 50 nm (Fig. 5b). The observed high particle size in DLS is attributed to the inclusion of bio-organic molecules surrounding the core of the ZnO-NPs. Additionally, the significant particle size may also result from the many forces of interaction in the solution, such as van der Waals interactions. The variations in particle sizes acquired using microscopic techniques are attributed to disparities in sample preparation and the polydispersity of the sample, as measured by DLS.

3.7 SEM

The surface morphology of the powder was analyzed using a scanning electron microscope. The rod-shaped nanoparticle exhibited porous characteristics and achieved a length of 50-60 nm. Prior research has demonstrated that ZnO in the form of rod structures exhibits superior optical characteristics. The ZnO crystals obtained from isopropanol exhibited a distinct morphology of elongated rods with a hexagonal cross-section. In contrast, the crystals obtained from ethanol had a less defined crystalline structure and appeared disc-like with a hexagonal cross-section (Vimala *et al.* 2014).

3.8 MTT Assay

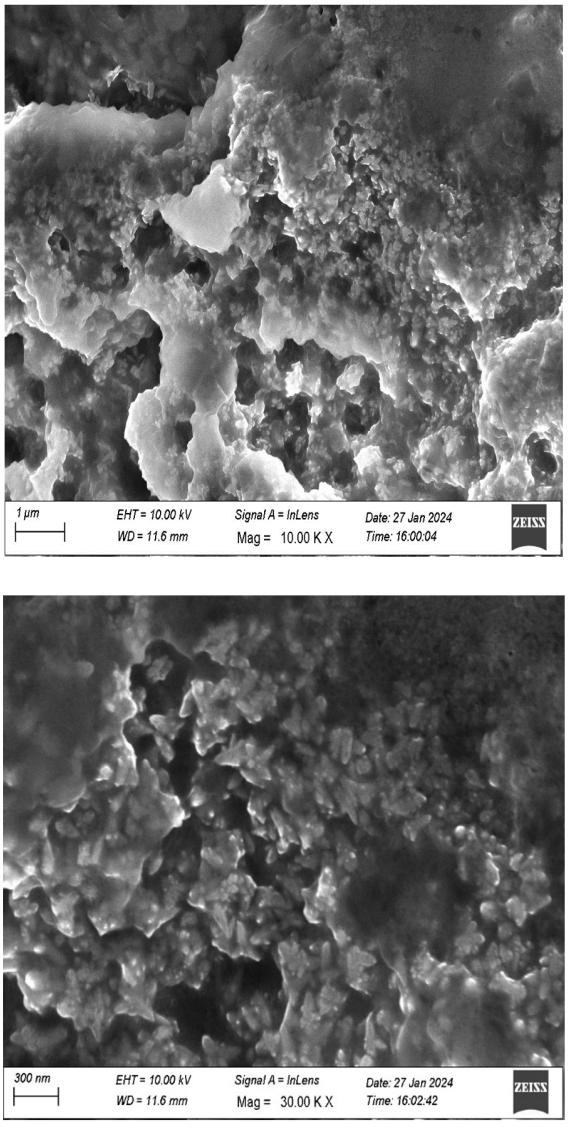


Fig. 6: SEM images of CB-ZnO-NPs

The effect of the CB-ZnO-NPs on the cell response of the human lung cancer cells was analyzed by MTT assay. Fig 7 shows the *in vitro* cytotoxicity activity of extract (up to 100µg/ml concentrations) against selected cancer cells. The experimental results demonstrate that the CB-ZnO-NPs inhibited cell proliferation in a dose dependent manner.

The IC_{50} values of ZnO-NPs, chavibetol and CB-ZnO-NPs against cancer cells were found to be 25, 21 and 9 µg/mL, respectively (Fig. 7). The observed IC_{50} values show that drug-loaded ZnO-NPs inhibit the proliferation of A549 human lung cancer cells. Vimala *et al.* (2014) reported that ZnO nanoparticles exhibit inherent cytotoxicity and significantly enhance the anticancer efficacy of DOX due to improved drug uptake and combined action. These findings support the present results.

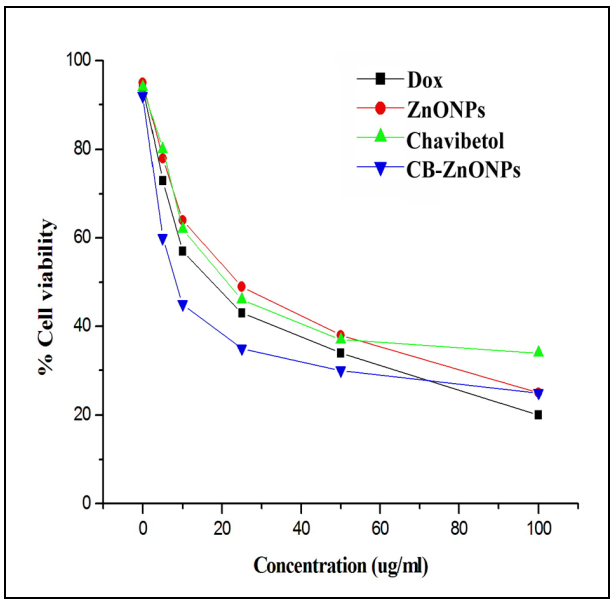


Fig. 7: Cytotoxic analysis of synthesized nanomaterials on Human Lung cancer cell (A549)

3.9 Cell Morphology Analysis

The morphological changes of selected cancer cells in the absence and presence of material at various concentrations are shown in Fig. 8-10. It could be observed that control cells did not show any remarkable changes in their morphology. However, in the presence of ZnO-NPs, chavibetol and CB-ZnO-NPs, the cells show improved cell shrinkage, membrane blebbing and floating cells in a dose-dependent manner. It is well accepted that cytological investigations elucidate the antiproliferative effect routed through membrane blebbing, membrane instability and distressing of the cytoskeleton of the cells by the CB-ZnO-NPs compared to chavibetol and ZnO-NPs alone. Based on the findings presented here, the CB-ZnO-NPs demonstrated anticancer capabilities. Multiple studies have shown that the production of reactive oxygen species (ROS) is a crucial mechanism by which zinc nanoparticles cause cell death.

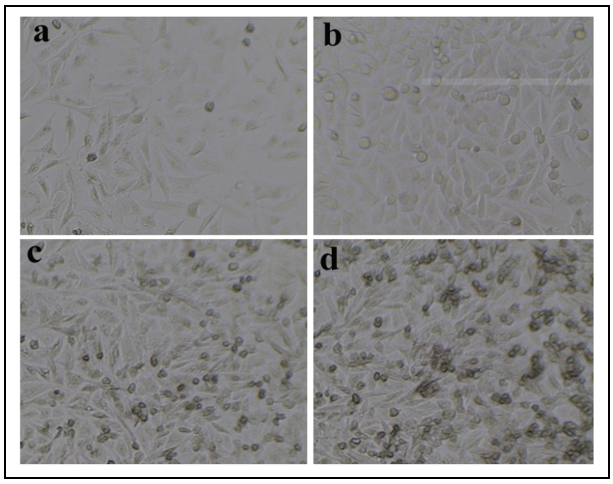


Fig. 8: Morphometric analysis of synthesized ZnO-NPs on A549 cells under phase contrast inverted microscope a) Control b) 5 µg/mL, c) 10 µg/mL and d) 25 µg/mL of ZnO-NPs treated cells

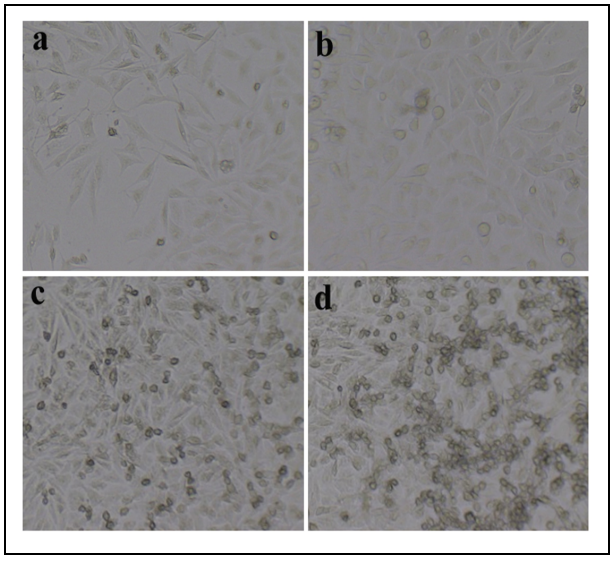


Fig. 9: Morphometric analysis of Chavibetol on A549 cells under phase contrast inverted microscope a) Control b) 5 µg/mL, c) 10 µg/mL and d) 25 µg/mL of chavibetol treated cells

Reactive oxygen species, including superoxide, hydroxyl radicals, and hydrogen peroxide, are continuously produced and removed in biological systems. Reactive oxygen species are widely recognized

for their significant contributions to various normal biochemical functions and abnormal disease processes. Oxidative stress occurs in cells when there is an excessive buildup of ROS that surpasses the capacity of the cellular antioxidant defense system. This leads to the impairment of cellular components such as lipids, proteins, and DNA.

3.10 Acridine Orange /Ethidium Bromide (AO/EtBr) Staining Method

Fluorescence microscopic analysis using AO/EtBr staining was performed to evaluate the apoptotic activity on A549 cells (Fig. 11–13). The control cells (a) in all figures exhibited normal morphology with uniform green fluorescence, indicating viable cells without significant damage. In contrast, cells treated with ZnO NPs (Fig. 11b–d), chavibetol (Fig. 12b–d), and CB–ZnO NPs (Fig. 13b–d) showed concentration-dependent morphological changes such as bright fluorescence, chromatin condensation, and nuclear fragmentation, confirming apoptosis. Among the tested samples, CB–ZnO NPs (Fig. 13) exhibited the most pronounced apoptotic features, followed by ZnO NPs (Fig. 11) and chavibetol (Fig. 12). The increased orange to red fluorescence in treated cells further indicates loss of membrane integrity and late-stage apoptosis.

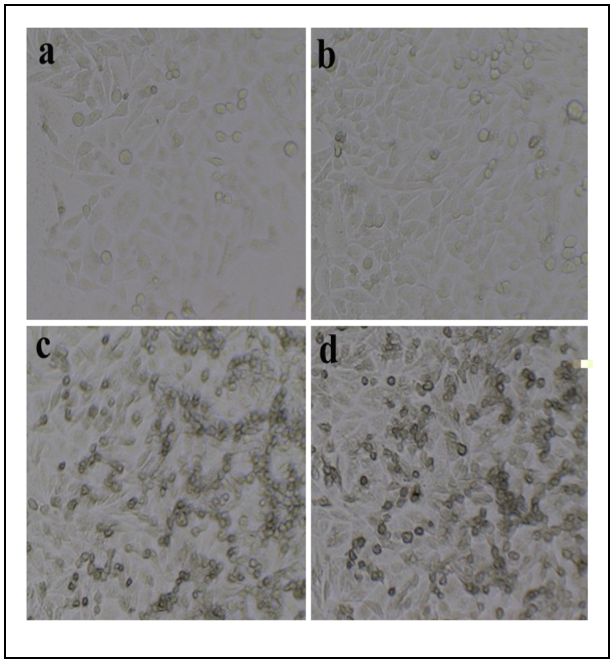


Fig. 10: Morphometric analysis of synthesized CB-ZnO-NPs on A549 cells under phase contrast inverted microscope a) Control b) 5 µg/mL, c) 10 µg/mL and d) 25 µg/mL of CB-ZnO-NPs treated cells

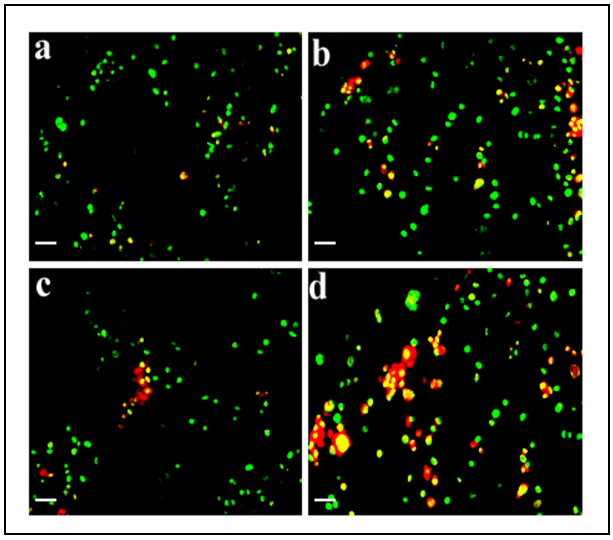


Fig. 11: AO/EtBr fluorescent analysis of synthesized ZnONPs on A549 cells under phase contrast inverted microscope a) Control b) 5 µg/mL, c) 10 µg/mL and d) 25 µg/mL ZnONPs treated cells. The scale bar measures about 50 µm

EtBr (red) stains apoptotic cells, while AO (green) marks viable cells. Control cells showed strong green fluorescence, confirming cell viability. Upon treatment with CB–ZnO NPs (5, 10, and 25 µg mL^{-1}), cells exhibited orange fluorescence (early apoptosis) and red fragmented nuclei (late apoptosis), indicating dose-dependent cell death. This effect is mainly associated with ROS generation, leading to lipid peroxidation, oxidative stress, and subsequent damage to cellular components such as DNA, proteins, and lipids, thereby triggering apoptosis.

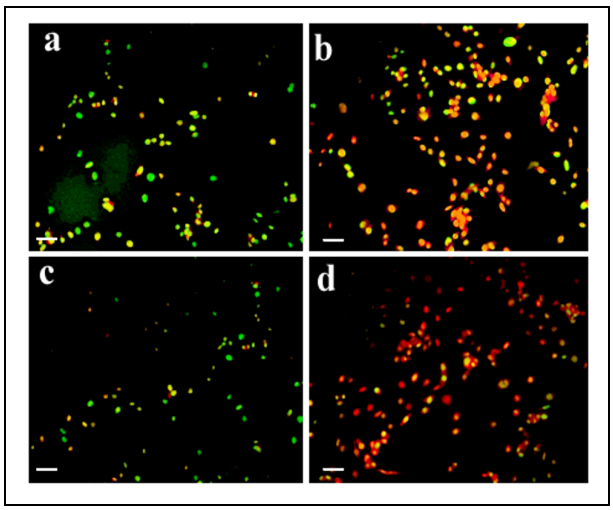


Fig. 12: AO/EtBr fluorescent analysis of synthesized chavibetol on A549 cells under phase contrast inverted microscope a) Control b) 5µg/ml, c) 10µg/ml, d) 25µg/ml chavibetol treated cells. The scale bar measures about 50µm

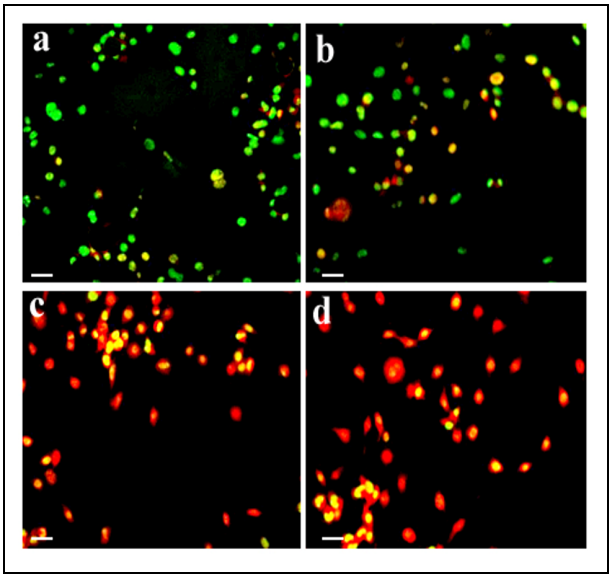


Fig. 13: AO/EtBr fluorescent analysis of synthesized CB-ZnONPs on A549 cells under phase contrast inverted microscope a) Control b) 5µg/ml, c) 10µg/ml, d) 25µg/ml chavibetol treated cells. The scale bar measures about 50µm

3.11 Protein Expression Analysis

Apoptosis is regulated by multiple proteins. Fig. 14 shows the expression of Bax, caspase-3, caspase-9, Bcl-2, and β-actin to elucidate the apoptotic pathway induced by CB–ZnO NPs. The results reveal dose-dependent upregulation of Bax, caspase-3, and caspase-9, while β-actin remained unchanged as an internal control. These findings suggest activation of the intrinsic apoptotic pathway, consistent with previous reports (Ahamed *et al.* 2012; Li *et al.* 2020).

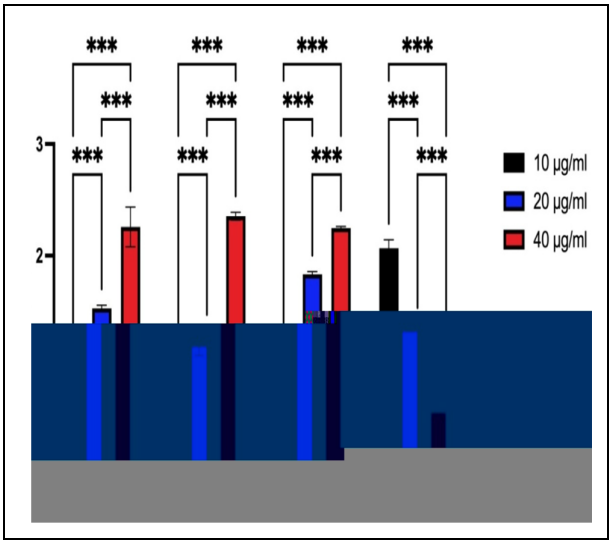


Fig. 14: Protein Expression analysis after treatment with the CB-ZnO-NPs in human lung cancer cells

4. CONCLUSION

Chavibetol-coated ZnO nanoparticles were successfully synthesized *via* a simple hydrothermal method, yielding highly crystalline and uniformly sized particles. The FTIR analysis confirmed effective conjugation of chavibetol onto ZnO nanoparticles. The system exhibited pH-responsive drug release, with higher release in acidic conditions. The composite demonstrated significant cytotoxicity and induced apoptosis in lung cancer cells through the intrinsic pathway, as supported by protein expression analysis. Thus, the nanoparticles effectively inhibited *in vitro* cancer cell growth, indicating their potential as a drug delivery system, though further *in vivo* studies are required.

FUNDING

This research received no specific grant from any funding agency in the public, commercial, or not-for-profit sectors.

CONFLICTS OF INTEREST

The authors declare that there is no conflict of interest.

COPYRIGHT

This article is an open-access article distributed under the terms and conditions of the Creative Commons Attribution (CC BY) license (http://creativecommons.org/licenses/by/4.0/).

REFERENCES

Aara, A., Chappidi, V. and Ramadas, M., Antioxidant activity of eugenol in Piper betel leaf extract, *J. Fam. Med. Prim. Care,* 9(1), 327 (2020). https://doi.org/10.4103/jfmpc.jfmpc_809_19

Abayarathne, H. M. I., Dunuweera, S. P. and Rajapakse, R. M. G., Synthesis of cisplatin encapsulated Zinc oxide nanoparticles and their application as a carrier in targeted drug delivery, *Ceylon J. Sci.,* 49(1), 71 (2020). https://doi.org/10.4038/cjs.v49i1.7707

Ahamed, M., Javed Akhtar, Kumar, Khan, M. and Ahmad, Alrokayan, Zinc oxide nanoparticles selectively induce apoptosis in human cancer cells through reactive oxygen species, *Int. J. Nanomed.*, 845 (2012). https://doi.org/10.2147/IJN.S29129

Aljabali, A. A. A., Obeid, M. A., Bakshi, H. A., Alshaer, W., Ennab, R. M., Al-Trad, B., Al Khateeb, W., Al-Batayneh, K. M., Al-Kadash, A., Alsotari, S., Nsairat, H. and Tambuwala, M. M., Synthesis, Characterization, and Assessment of Anti-Cancer Potential of ZnO Nanoparticles in an In Vitro Model of Breast Cancer, *Molecules,* 27(6), 1827 (2022). https://doi.org/10.3390/molecules27061827

Alrushaid, N., Khan, F. A., Al-Suhaimi, E. A. and Elaissari, A., Nanotechnology in Cancer Diagnosis and Treatment, *Pharmaceutics,* 15(3), 1025 (2023). https://doi.org/10.3390/pharmaceutics15031025

Anjum, S., Hashim, M., Malik, S. A., Khan, M., Lorenzo, J. M., Abbasi, B. H. and Hano, C., Recent Advances in Zinc Oxide Nanoparticles (ZnO NPs) for Cancer Diagnosis, Target Drug Delivery, and Treatment, *Cancers (Basel),* 13(18), 4570 (2021). https://doi.org/10.3390/cancers13184570

Asif, N., Amir, M. and Fatma, T., Recent advances in the synthesis, characterization and biomedical applications of zinc oxide nanoparticles, *Bioprocess Biosyst. Eng.,* 46(10), 1377–1398 (2023). https://doi.org/10.1007/s00449-023-02886-1

Baranwal, J., Barse, B., Di Petrillo, A., Gatto, G., Pilia, L. and Kumar, A., Nanoparticles in Cancer Diagnosis and Treatment, *Mater. (Basel),* 16(15), 5354 (2023). https://doi.org/10.3390/ma16155354

Halanayake, K. D., Kalutharage, N. K. and Hewage, J. W., Microencapsulation of biosynthesized zinc oxide nanoparticles (ZnO-NPs) using Plumeria leaf extract and kinetic studies in the release of ZnO-NPs from microcapsules, *SN Appl. Sci.,* 3(1), 17 (2021). https://doi.org/10.1007/s42452-020-04100-3

Jin, S. E. and Jin, H. E., Synthesis, Characterization, and Three-Dimensional Structure Generation of Zinc Oxide-Based Nanomedicine for Biomedical Applications, *Pharmaceutics.,* 11(11), 575 (2019). https://doi.org/10.3390/pharmaceutics11110575

Kulothungan, V., Sathishkumar, K., Leburu, S., Ramamoorthy, T., Stephen, S., Basavarajappa, D., Tomy, N., Mohan, R., Menon, G. R. and Mathur, P., Burden of cancers in India - estimates of cancer crude incidence, YLLs, YLDs and DALYs for 2021 and 2025 based on National Cancer Registry Program, *BMC Cancer,* 22(1), 527 (2022). https://doi.org/10.1186/s12885-022-09578-1

Li, J., He, J., Huang, Y., Li, D. and Chen, X., Improving surface and mechanical properties of alginate films by using ethanol as a co-solvent during external gelation, *Carbohydr. Polym.,* 123, 208–216 (2015). https://doi.org/10.1016/j.carbpol.2015.01.040

Li, Z., Guo, D., Yin, X., Ding, S., Shen, M., Zhang, R., Wang, Y. and Xu, R., Zinc oxide nanoparticles induce human multiple myeloma cell death via reactive oxygen species and Cyt-C/Apaf-1/Caspase-9/Caspase-3 signaling pathway in vitro, *Biomed. Pharmacother,* 122, 109712 (2020). https://doi.org/10.1016/j.biopha.2019.109712

Martínez, C. M., Gun'ko, Y. and Vallet-Regí, M., ZnO Nanostructures for Drug Delivery and Theranostic Applications, *Nanomaterials,* 8(4), 268 (2018). https://doi.org/10.3390/nano8040268

Nishida, N., Yano, H., Nishida, T., Kamura, T. and Kojiro, M., Angiogenesis in cancer, *Vasc. Health Risk Manag.,* 2(3), 213–219 (2006). https://doi.org/10.2147/vhrm.2006.2.3.213

Pang, R. W. and Poon, R. T., Clinical implications of angiogenesis in cancers, *Vasc. Health Risk Manag.,* 2(2), 97–108 (2006). https://doi.org/10.2147/vhrm.2006.2.2.97

Saddik, M. S., Elsayed, M. M. A., El-Mokhtar, M. A., Sedky, H., Abdel-Aleem, J. A., Abu-Dief, A. M., Al-Hakkani, M. F., Hussein, H. L., Al-Shelkamy, S. A., Meligy, F. Y., Khames, A. and Abou-Taleb, H. A., Tailoring of Novel Azithromycin-Loaded Zinc Oxide Nanoparticles for Wound Healing, *Pharma.,* 14(1), 111 (2022). https://doi.org/10.3390/pharmaceutics14010111

Shah, S. C., Kayamba, V., Peek, R. M. and Heimburger, D., Cancer Control in Low- and Middle-Income Countries: Is It Time to Consider Screening?, *J. Glob. Oncol.,* (5), 1–8 (2019). https://doi.org/10.1200/JGO.18.00200

Siddiqi, K. S., ur-Rahman, A. and Tajuddin, H. A., Properties of Zinc Oxide Nanoparticles and Their Activity Against Microbes, *Nanoscale Res. Lett.,* 13(1), 141 (2018). https://doi.org/10.1186/s11671-018-2532-3

Tran, K. A., Kondrashova, O., Bradley, A., Williams, E. D., Pearson, J. V. and Waddell, N., Deep learning in cancer diagnosis, prognosis and treatment selection, *Genome Med.,* 13(1), 152 (2021). https://doi.org/10.1186/s13073-021-00968-x

Vimala, K., Sundarraj, S., Paulpandi, M., Vengatesan, S. and Kannan, S., Green synthesized doxorubicin loaded zinc oxide nanoparticles regulates the Bax and Bcl-2 expression in breast and colon carcinoma, *Process Biochem.,* 49(1), 160–172 (2014). https://doi.org/10.1016/j.procbio.2013.10.007